Supplementary Data Table of Contents

Supplemental Figures

Supplementary Figure 1 (A-D) – CHIP expression in the heart. (**A**) Immunoblot analysis of CHIP expression in neonatal primary cardiomyocytes (CM) and non-cardiomyocyte cells (Non) derived from 129SvEv mouse hearts. The specificity of the CHIP antibody was confirmed using MEF cells isolated from either wild-type (WT) or *CHIP* $^{-/-}$ (KO) mice and equal loading of the MEF samples confirmed by immunodetection of βACTIN. (**B**) Indirect immunofluorescence of CHIP (upper) and cardiac troponin C (TnC, lower) in heart sections from 129SvEv mice. DAPI was used as a nuclear counterstain (middle) and differential interference contrast (DIC) was used to enhance the contrast of the color overlays (right). Scale bar represents 50 microns. (**C**) High power magnification of the region outlined in (**B**). The open and closed arrows indicate CHIP or TnC expression, respectively, localized in identical regions of the sarcomere within cardiomyocytes. The circled regions identify increased regions of CHIP expression surrounding or within the nucleus of cardiomyocytes. Scale bar represents 50 microns. (**D**) To rule out non-specific cross-reaction of the secondary antibodies confounding the localization patterns of CHIP (mouse IgG2b) and TnC (mouse IgG2a) antibodies, the secondary antibodies were mismatched, using anti-mouse IgG2a and anti-mouse IgG2b, respectively. Additionally, there was no signal above background fluorescence in heart sections from *CHIP* $^{-/-}$ mice to ensure specificity of the CHIP antibody (data not shown).

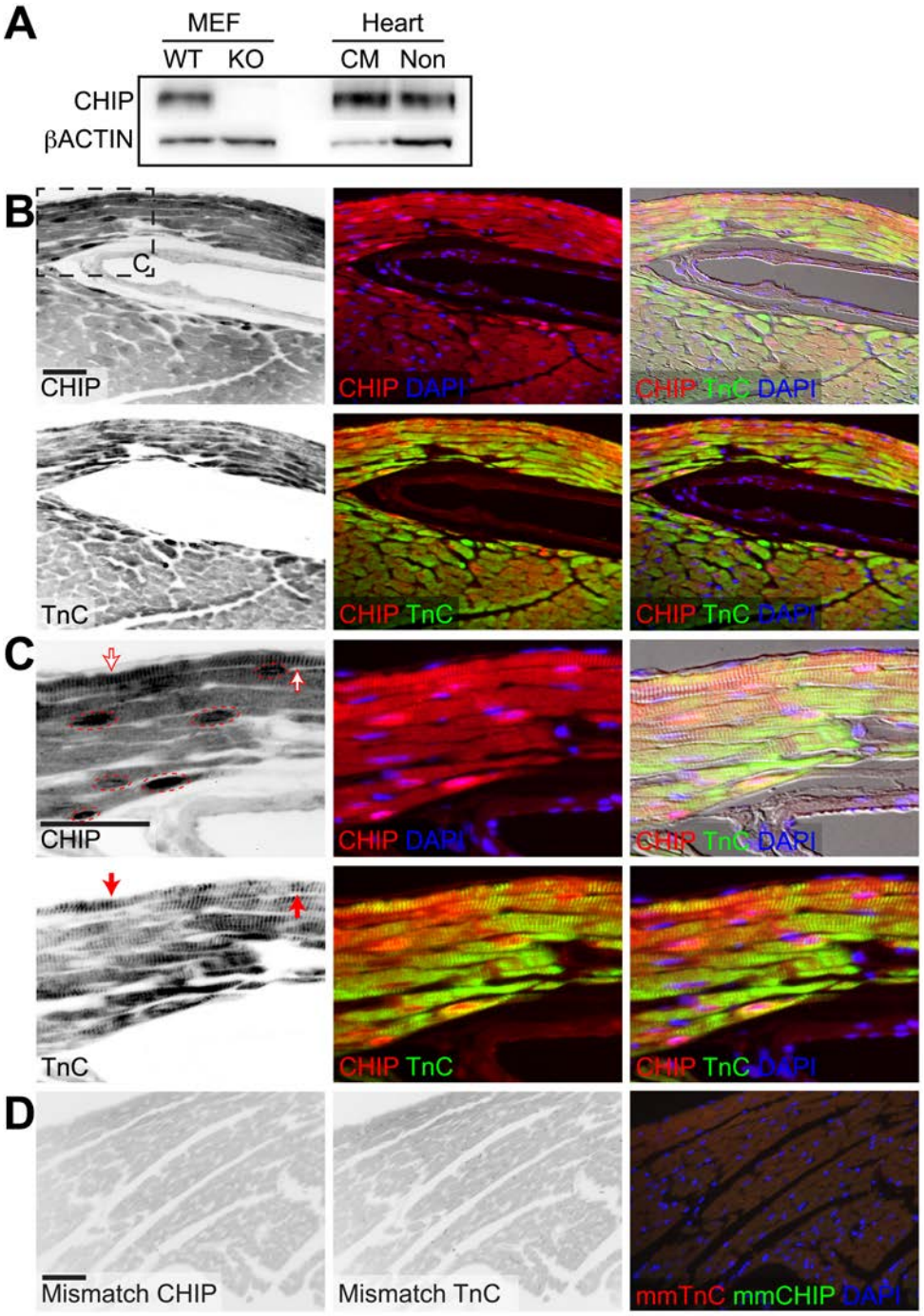

Supplementary Figure 1 A-D Schisler *et al.*

Supplementary Figure 1 (E-G) – Interstitial fibrosis in mouse heart sections. (**E**) Low power magnification of whole heart sections from wild-type and *CHIP* $^{-/-}$ mice subjected to TAB surgery stained with Masson's-Trichrome to indicate fibrosis. Scale bar represents 500 microns. (**F**) A representative threshold image used to calculate the amount of fibrosis in each heart section is provided. The ventricle area was first identified and selected (RAW, left) allowing the area of fibrosis (blue) and total area (red plus blue) to be quantified (Trichrome Threshold, right). Scale bar represents 500 microns. (**G**) Quantification of the percent interstitial fibrosis (area of fibrosis/total area) in banded wild-type or *CHIP* $^{-/-}$ mouse hearts are represented by the mean ± SEM (n = 11 or 13 whole heart sections, respectively: *** $p < 0.0001$ using student's t-test).

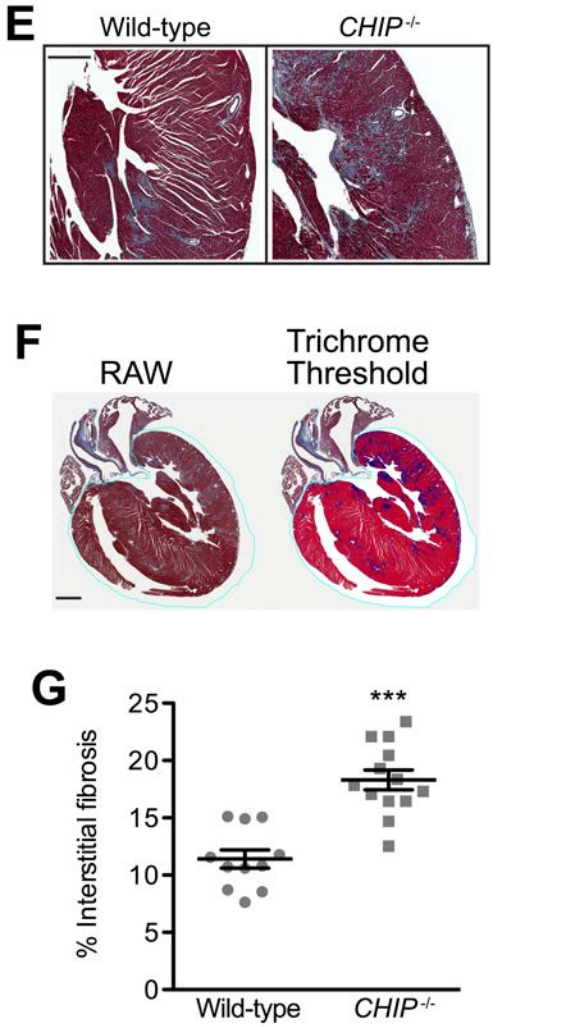

Supplementary Figure 1 E-G Schisler *et al.*

Supplementary Figure 2 (A-D) – Mitochondrial volume density and microarray analysis of gene expression in banded wild-type and CHIP -/- mouse hearts. (**A**) Electron micrographs from wild-type and *CHIP* $^{-/-}$ mouse hearts after one week of TAB or sham surgery were used to quantify the mitochondrial volume density and are depicted as either a scatter plot (**left**) or a bar graph (**right**). Data are represented by the mean ± SEM (n = 13-30 micrographs representing at least 5 animals per condition, data are significant via 2-way ANOVA on the interaction between genotype and surgery at $p < 0.0001$; Bonferroni post-tests: ### $p < 0.001$ TAB vs. sham, ††† $p < 0.001$ wild-type vs. *CHIP* $^{-/-}$ after one week of TAB). (**B**) Principal component analysis (PCA) of global changes in cardaic gene expression was performed on the gene expression profiles of wild-type and *CHIP* $^{-/-}$ mice after one week following sham surgery or TAB represented by a scatter plot of the first (PC1) versus second principal component (PC2). Probes included for the PCA analysis met the following criteria - acceptable flags (present or marginal) in at least half of the biological replicates in one out of the four conditions (14,322 probes). PCA of the four conditions demonstrate that the first principle component (accounting for 64% of the variance) was largely attributed to the surgery condition (sham versus TAB) whereas the second component separated the wild-type from the *CHIP* $^{-/-}$ in the TAB condition (16% of the total variance) suggesting that the differences in gene expression after TAB were not attributed to baseline differences in gene expression. Four eigenvectors were calculated for PCA and data represented in the scatter plot are scaled to unit standard deviation. The confidence ellipses represent two standard deviations. (**C**) K-means and functional clustering of microarray analysis. K-means clustering of 168 probes corresponding to 160 differentially-expressed genes in hearts from wild-type and *CHIP* $^{-/-}$ mice in either sham or TAB conditions (left, n = 4 biological replicates per condition: 2-way ANOVA, corrected $p < 0.05$) results in three distinct clusters that span diverse myocyte functional pathways and locales (right). The normalized mean expression value of each cluster across the four biological replicates is indicated by the highlighted line (yellow). The genes from each cluster were classified for functional classification and over-representation and are represented by the fold enrichment (FE) value. The fold-enrichment

represents the multiple of enrichment for genes from the cluster compared to all the genes represented on the microarray for each functional class (middle, $p < 0.05$, see also Supplementary Table 2). (**D**) The 168 probes corresponding to 160 differentially-expressed genes in hearts from wild-type and *CHIP* $^{-/-}$ mice in either sham and TAB were clustered with average linkages using Pearson correlated centered metrics (Cluster 3.0, University of Tokyo, Human Genome Center) and represented by a heatmap. The colored and numbered clusters approximate the same clusters identified via K-means analysis (**C**).

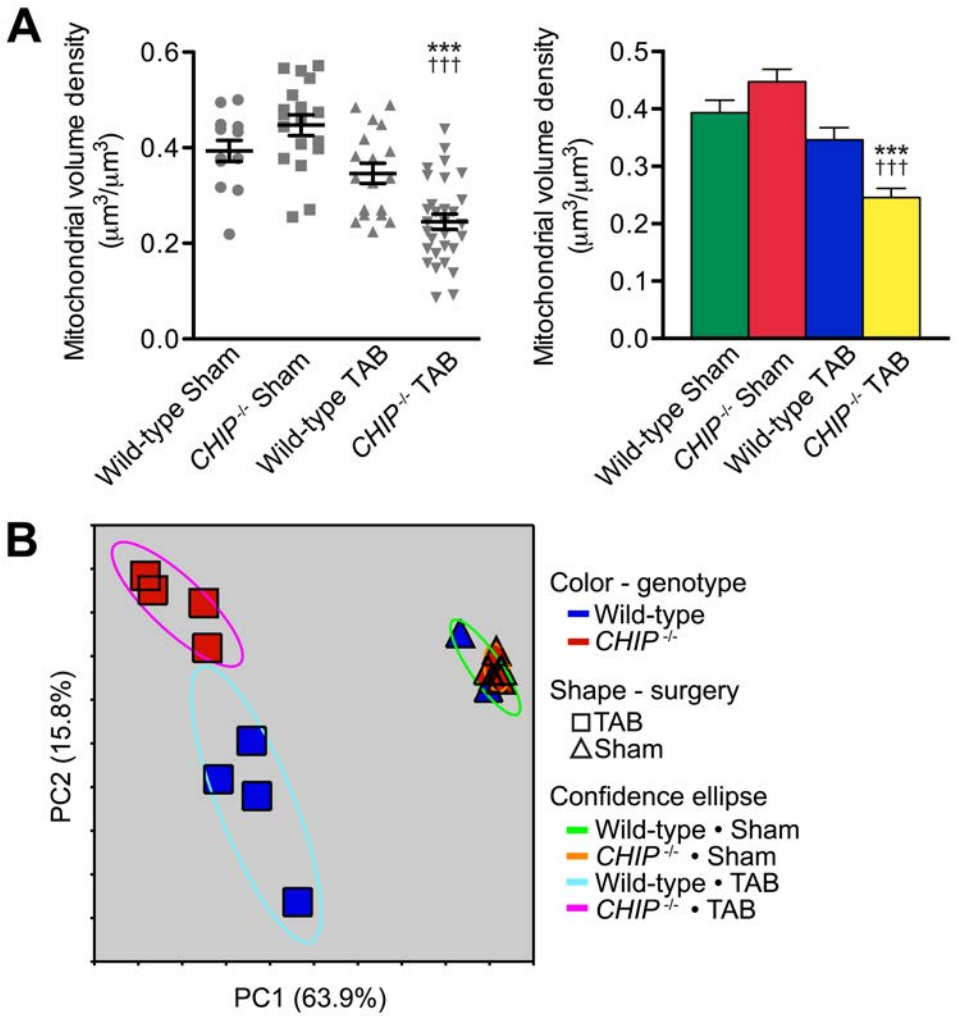

Supplementary Figure 2 A-B

Schisler *et al.*

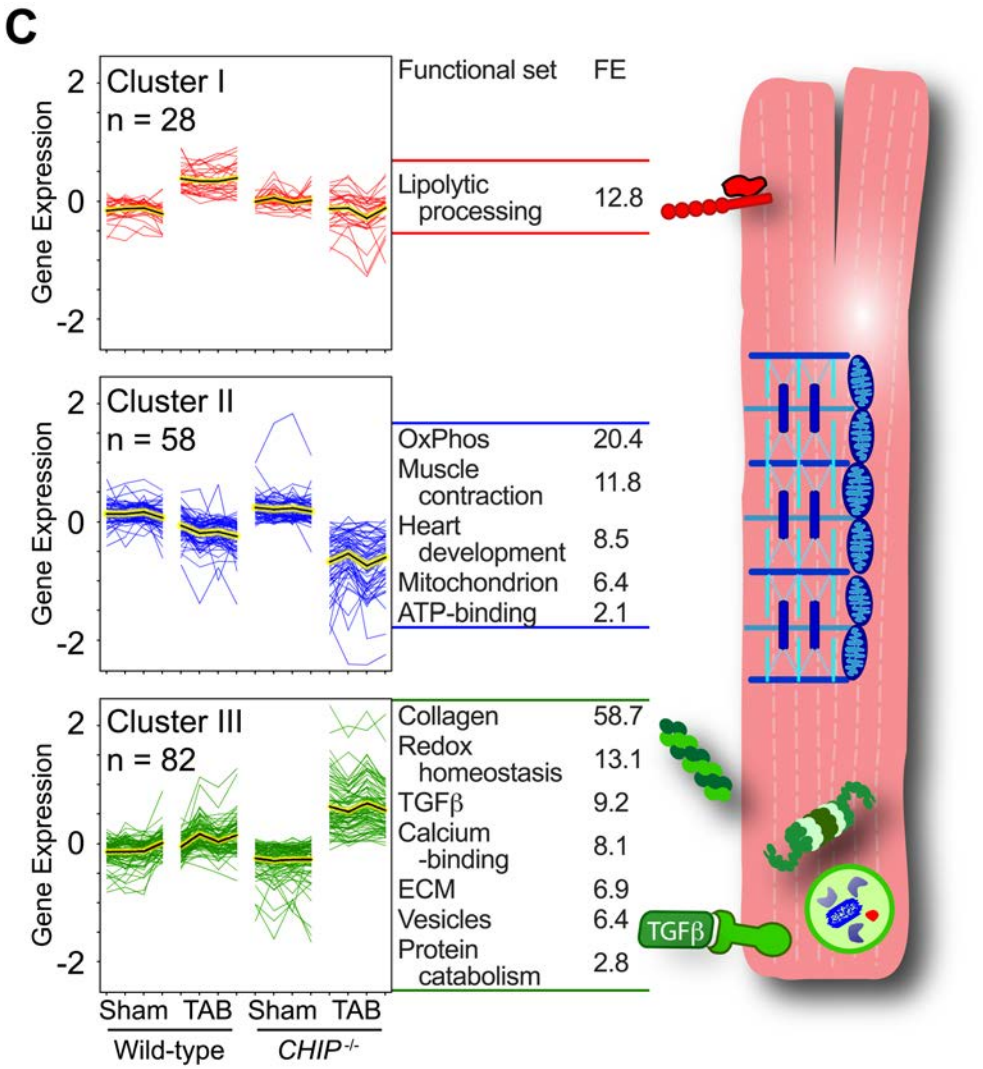

Supplemental Figure 2 C

Schisler *et al.*

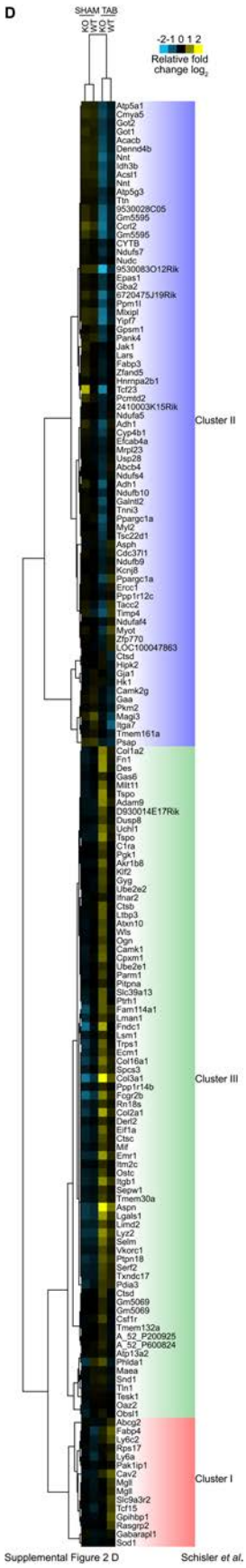
D
SHAM TAB
KO1
KO2
WT1
-2-1 0 1 2
Relative fold change log2
Cluster II
Cluster III
Cluster I
Supplemental Figure 2 D
Schisler et al.

Supplementary Figure 2 (E-G) – Reference gene fitness analysis for qPCR and qPCR validation of microarray analysis. Intergroup variation (*variation between groups*) plotted for genotype (**E**) and surgery (**F**) classifiers with intragroup variation (*variation within same group*) indicated by the vertical bars reflecting a confidence interval for the difference. Reference genes with intergroup variation > 0 implies systematically higher expression in both *CHIP* $^{-/-}$ and TAB surgery groups, whereas variation < 0 implies the opposite, also see Supplementary Table 3 & 4. (**G**) Oxidative phosphorylation (OxPhos) occurs over five multimeric complexes (upper): complex I (NADH dehydrogenase – green); complex II (Succinate dehydrogenase – light blue); complex III (Cytochrome c reductase – red); complex IV (Cytochrome c oxidase – purple); and ATP synthase (dark blue). Log_2 of mean-centered mRNA levels of various OxPhos transcripts initially identified via microarray analysis (Supplementary Fig. 2C, 2D, and Supplementary Table 2) were measured in mouse hearts via qPCR and represented by the mean ± SEM from four biological replicates per condition (lower, significant interaction between surgery and genotype: * $p < 0.05$, ** $p < 0.01$; post-test: † $p < 0.05$, †† $p < 0.01$ in wild-type vs *CHIP* $^{-/-}$ at one week of TAB) The mRNA labels are colored according to complex location.

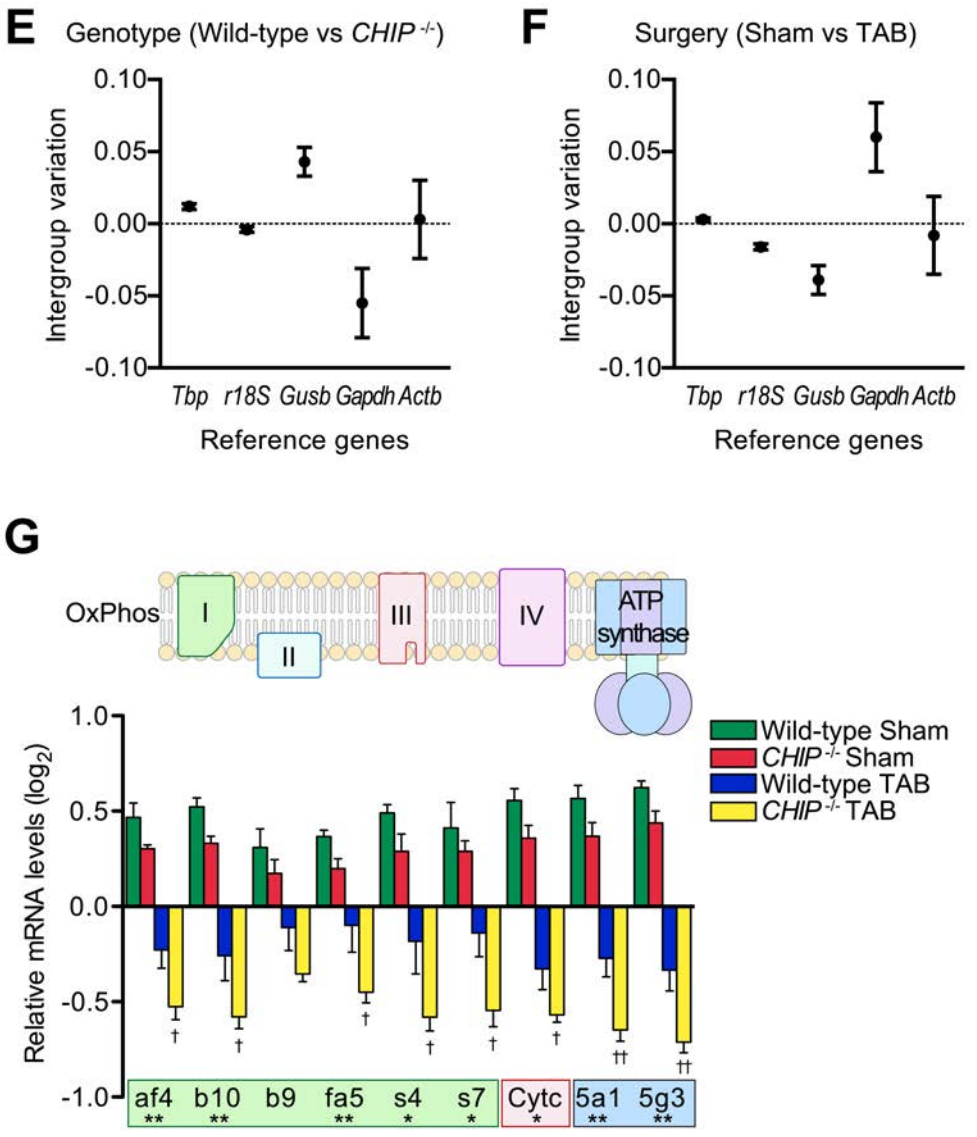

Supplemental Figure 2 E-G

Schisler *et al.*

Supplementary Figure 3 (A-C) – CHIP expression, phosphorylation of AMPK, cardiac AMPK activity, and candidate cardiac protein expression during pressure overload in mice. (**A**) Immunoblot (upper) and densitometry (lower) analysis of pAMPKα-T172 and CHIP expression in mouse hearts from wild-type mice at baseline and at one and four weeks after TAB surgery. Changes in pAMPKα-T172 and CHIP densitometry are represented by the mean ± SEM from three biological replicates per condition and were significant via ANOVA at $p < 0.05$; post-test * and † $p < 0.05$ comparing four week TAB to one week TAB or baseline, respectively. (**B**) Cardiac AMPKα1 and AMPKα2 activity in wild-type mice at baseline and at one and four weeks after TAB surgery measured by SAMS peptide phosphorylation in immunoprecipitants from mouse hearts. Activities for AMPKα1 and AMPKα2 were each normalized to baseline activity. Changes in cardiac AMPKα1 and AMPKα2 activities were significant via ANOVA at $p < 0.01$ and $p < 0.05$, respectively; post-test * $p < 0.05$ comparing AMPKα1 activity after four week TAB to either one week TAB or baseline, and † $p < 0.05$ comparing AMPKα2 activity after four week TAB to one week TAB. (**C**) Immunoblots and densitometry analysis of ERRα protein (left) or SGK1, pSGK1-S255/T256, HSP90, and HSP70 (right) after sham or TAB surgery. Relative cardiac protein levels normalized to GAPDH are expressed as mean ± SEM from three biological replicates per condition, significant interactions between surgery and genotype: * $p < 0.05$, ** $p < 0.01$; post-test: # $p < 0.05$, ### $p < 0.001$ in sham vs TAB surgery; † $p < 0.05$, †† $p < 0.01$ in *CHIP* $^{-/-}$ vs wild-type genotypes.

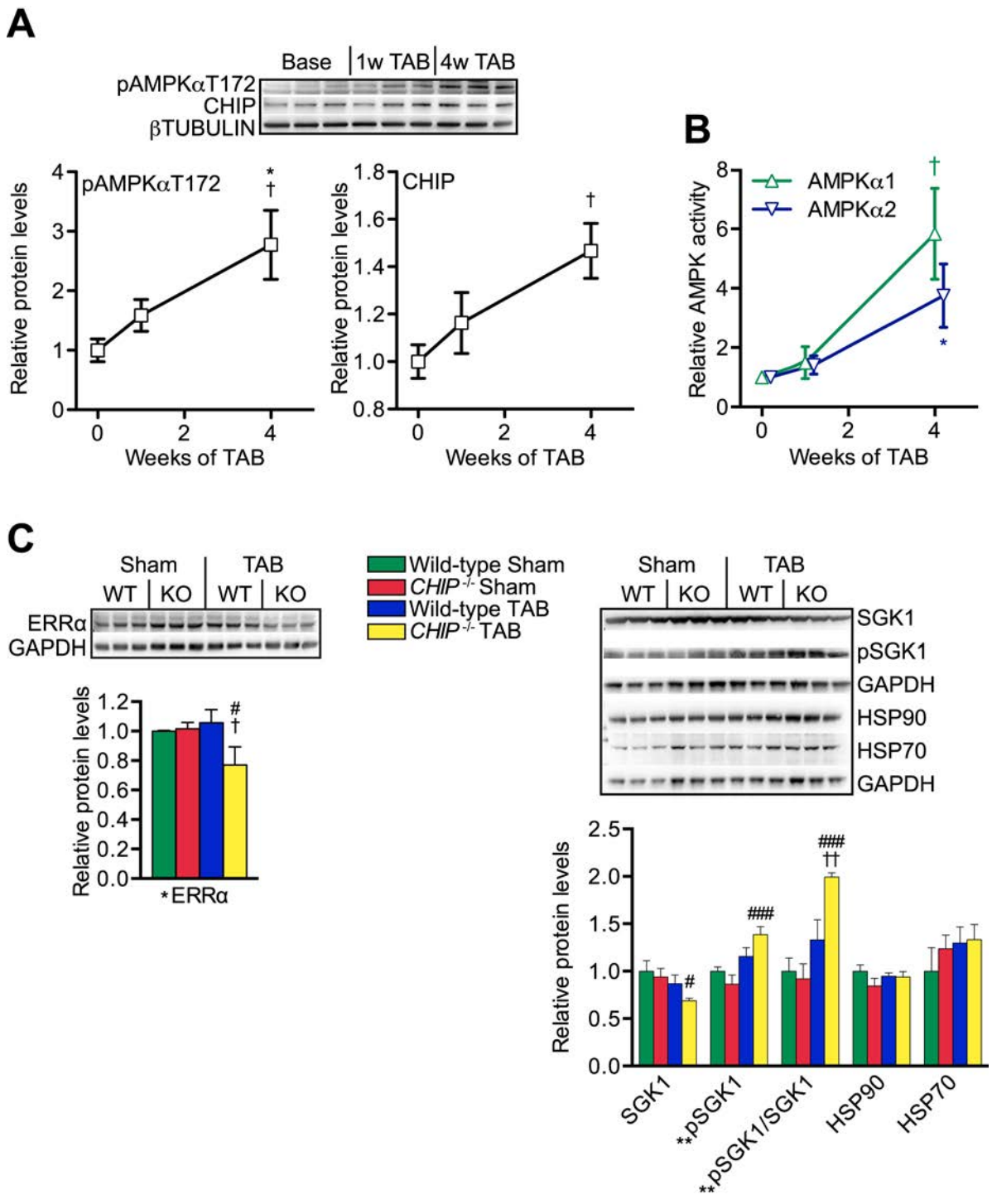

Supplementary Figure 3 A-C

Schisler *et al.*

Supplementary Figure 3 (D-E) – CHIP expression is necessary for oxidative stress-mediated AMPK activity in MEFs and AICAR-mediated activation of AMPK in mouse hearts.

(**D**) AMPK activity measured by SAMS phosphorylation (pSAMS) in immunoprecipitants from MEF lysates using a pan-AMPKα antibody. Cells were treated as described in Figure 3E and pSAMS is represented by the mean ± SEM from three biological replicates per condition (significant via two-tailed student's t-test comparing control (Ctl) and H_2O_2 paired conditions: * $p < 0.05$ and ** $p < 0.01$, ns = not significant at $p < 0.05$). (**E**) Representative immunoblots (upper) and densitometry analysis (lower) of pACC-S79, pAMPKα-T172, AMPKα, and CHIP expression in heart protein extracts after 72 h of treatment with either saline or AICAR in wild-type or *CHIP* $^{-/-}$ mice (WT or KO, respectively). Relative protein expression was normalized using GAPDH protein levels (n = 8 WT/saline, 5 $^{-/-}$/saline, 7 WT/AICAR, 5 $^{-/-}$/AICAR; Bonferroni post-tests of 2-way ANOVA on AICAR and genotype variables: ** $p < 0.01$, *** $p < 0.001$, mean ± SEM, nd = not detected). It is important to note that the amount of expression of adenosine kinase, the rate-limiting enzyme in AICAR metabolism is not changed in *CHIP* $^{-/-}$ mouse hearts compared to wild-type hearts, as determined by microarray analysis (fold change = 0.97 comparing *CHIP* $^{-/-}$ to wild-type hearts, corrected $p = 0.19$).

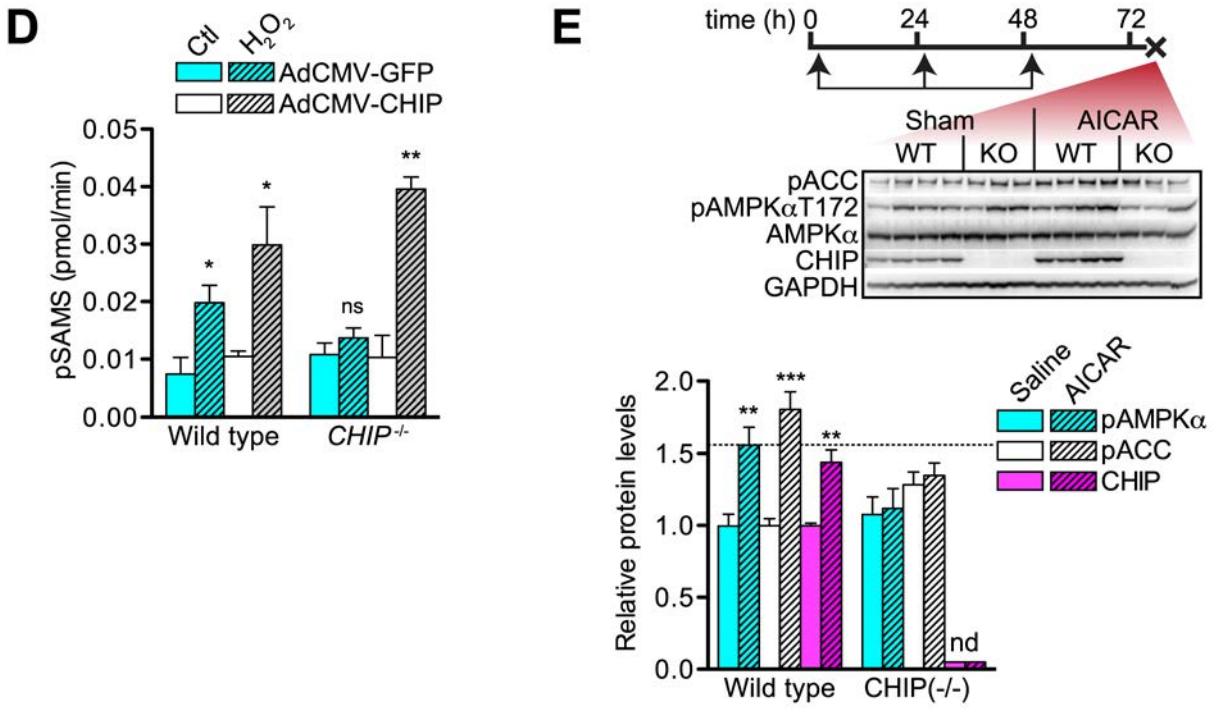

Supplementary Figure 3 D-E

Schisler *et al.*

Supplementary Figure 4 (A-B) – Co-immunoprecipitation analysis of CHIP and AMPK. (**A**) Results of the co-precipitation of AMPKγ1 with CHIP immunoprecipitation, see Figure 4A. We clearly observed AMPKγ1 co-immunoprecipitation with CHIP in wild-type mice (WT) however there is some non-specific co-immunoprecipitation as evident by the non-specific band observed in the *CHIP* $^{-/-}$ sample (KO). (**B**) Representative immunoprecipitations (IP) from wild-type heart lysates using goat antibodies against either AMPKα1 or AMPKα2, a mouse monoclonal antibody against CHIP, as well as goat (Gt) and mouse (Mus) IgG controls, subsequently immunoblotted (IB) for either pAMPKα-T172 or CHIP.

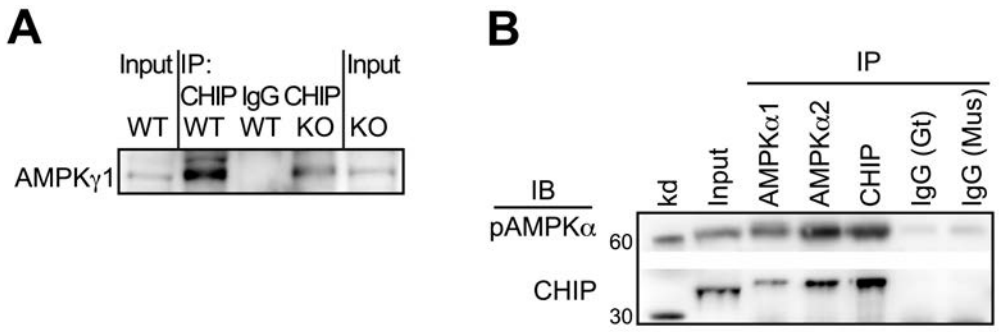

Supplemental Figure 4 A-B

Schisler *et al.*

Supplementary Figure 4 (C-F) – Stoichiometry analysis of the CHIP-AMPK reveals a stable complex of a CHIP dimer with the AMPK trimeric holoenzyme. CHIP exists primarily as a homodimer of ≈70 kd whereas the AMPK holoenzyme is a complex of ≈140 kd. Additionally, both proteins form higher order multimers (1, 2) (**C**) Native-PAGE/immunoblot analysis of recombinant AMPKα2β1γ1 in the absence or presence of increasing amount of recombinant CHIP protein (+, ++, and +++ indicate molar ratios of CHIP:AMPK of 0.5:1, 2:1, and 4;1, respectively) detected with antibodies (IB) for either CHIP (left) or AMPKα2 (right). Molecular mass markers (kd) are provided; the red, black, and white arrows indicate the CHIP dimer, AMPKα2β1γ1 holoenzyme, and the CHIP-AMPK complex, respectively. The same protein complex formation and stoichiometry was seen with AMPKα1β1γ1 and CHIP, data not shown. (**D**) Two dimensional native-PAGE/SDS-PAGE of AMPKα2β1γ1 ('A') in the absence or presence of CHIP ('C'). Recombinant proteins and the complexes formed were resolved in the first dimension using native-PAGE (1° NATIVE) as shown in (**C**). The native-PAGE bands were excised and run on a reducing SDS-PAGE gel (2° SDS) resolving the reduced proteins. The molecular mass markers of both dimensions are provided. As shown in (**C**), the red, black, and white arrows indicate the CHIP dimer, AMPKα2β1γ1 holoenzyme, and the CHIP-AMPK complex, respectively. (**E**) Native-PAGE/immunoblot analysis of recombinant activated (phosphorylated αT172) pAMPKα2β1γ1 holoenzyme in the absence or presence of increasing amount of recombinant CHIP protein detected with an AMPKα2 antibody. Molecular mass markers (kd) are provided; the black and white arrows indicate the pAMPKα2β1γ1 holoenzyme and the CHIP-AMPK complex, respectively. Equally, the same protein complex formation and stoichiometry was observed with activated (phosphorylated αT172) pAMPKα1β1γ1 and CHIP, data not shown. (**F**) Size-exclusion chromatography multi-angle light scattering (SEC-MALS) of recombinant CHIP (blue), AMPKα2β1γ1 (brown) and a combination of AMPKα2β1γ1 and CHIP (purple). The single protein mixtures were run at 1 mg/ml, and the combination reaction contained 1 mg/ml of AMPKα2β1γ1 and 0.5 mg/ml of CHIP. The molecular mass of each peak

(Y-axis, diamond data points) and the hydrodynamic radius (spheres) are superimposed on the Rayleigh ratio chromatographs that represent the amount of light scattering.

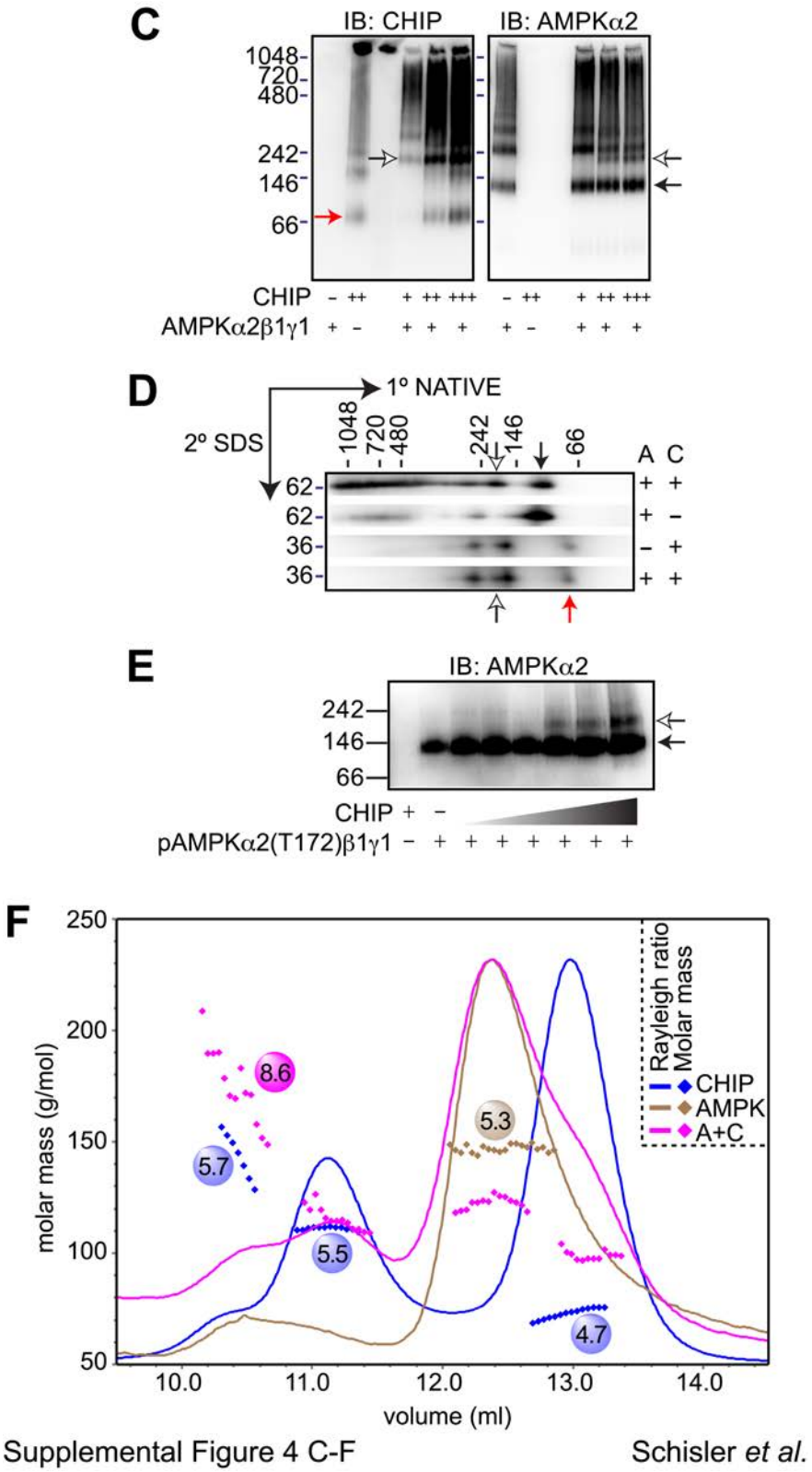

Supplemental Figure 4 C-F Schisler *et al.*

Supplementary Figure 4 (G-H) – Functional analysis of the CHIP-AMPK interaction. (**G**) Representative immunoblot analysis (upper) of pAMPKα-T172, MOD25α (LKB1), and CHIP expression and densitometry analysis (lower) of pAMPKα-T172 expression at baseline (0 m) or at 10 and 30 m at 30 °C after the addition of recombinant LKB1/STRADα/MO25α to reactions containing unphosphorylated monomeric AMPKα2 in the absence (control) or presence of wild-type CHIP protein, or two mutant CHIP proteins (K30A, ΔU-box). The amount of phosphorylated AMPKα-T172 is expressed as mean ± SEM (n = 3 independent experiments, significant via ANOVA at 10 and 30 m, at $p < 0.001$ and $p < 0.0001$, respectively; * $p < 0.05$ and ** $p < 0.01$ vs. control condition at each time point). (**H**) Representative immunoblot and densitometry analysis (upper) of pAMPKα-T172 levels normalized to AMPKβ and AMPK-specific activity (lower) measured in reactions containing combinations of activated (phosphorylated αT172) pAMPKα1β1γ1 (left) and pAMPKα2β1γ1 (right), CHIP, and AMP as indicated followed by treatment with or without PP2Cα for 30 m. There were no significant differences in the amount of pAMPKα-T172 comparing paired conditions in the presence or absence of CHIP. Data are expressed as mean ± SEM from three biological replicates per condition, significant by ANOVA: post-test †† $p < 0.01$ and ††† $p < 0.001$ comparing the respective control condition (-AMP/-PP2Cα, or +AMP/-PP2Cα); ‡ $p < 0.05$, ‡‡ $p < 0.01$, and ‡‡‡ $p < 0.001$ comparing reactions ±AMP in the presence of PP2Cα; *** $p < 0.001$ in the presence of CHIP.

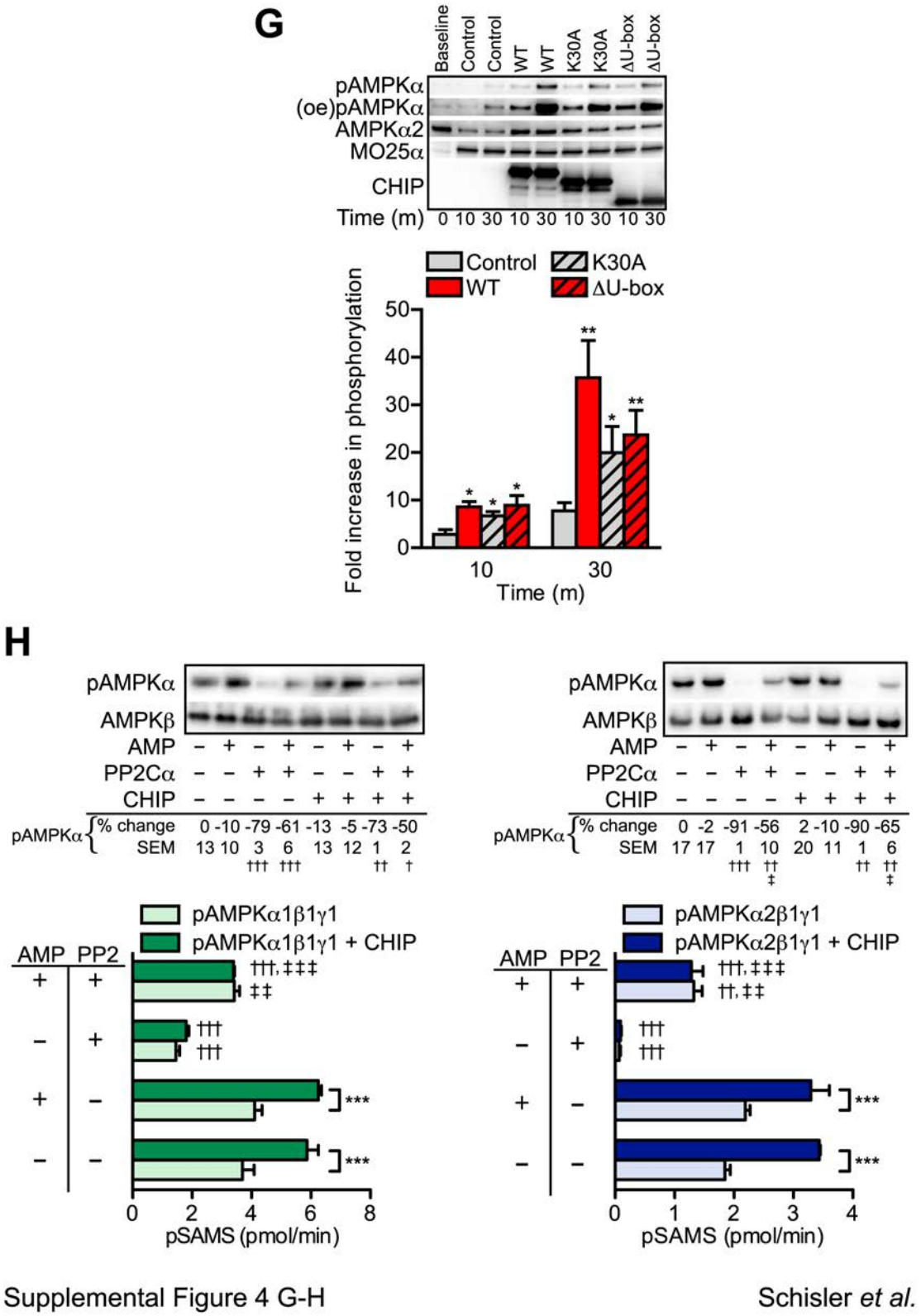

Supplemental Figure 4 G-H

Schisler *et al.*

Supplementary Figure 4 (I-J) – CHIP increases AMPK activity. (**I**) Activated (phosphorylated αT172) pAMPKα1 (left, green) and pAMPKα2 (right, blue) phosphorylation levels and kinase activity in reactions where CHIP is either excluded (no CHIP), added 10 m before (pre CHIP), or at the end (post CHIP) of the AMPK activity assay measured by SAMS phosphorylation (pSAMS). Phosphorylation of AMPKα-T172 and total AMPKα was determined via immuno-slotblotting analysis. There was no difference in the amount of phosphorylated AMPKα-T172 or total AMPKα across the three conditions. Changes in pAMPKα1 and pAMPKα2 activity are represented by mean ± SEM from three biological replicates per condition and are significant via ANOVA: *** $p < 0.001$ and $p < 0.0001$, respectively. (**J**) AMPK-specific activity represented by mean ± SEM in purified recombinant protein mixtures containing either activated (phosphorylated αT172) pAMPKα1β1γ1 (green) or pAMPKα2β1γ1 (blue) mixed with increasing amounts of recombinant CHIP (open circles) or IgG (closed circles). The molar ratios between CHIP and pAMPK for each concentration of CHIP are provided (red text). The hashed green and blue lines indicate baseline-specific activities of pAMPKα1- and pAMPKα2-containing complexes in the absence of other proteins, respectively (n = 3 independent *in vitro* experiments, one-tailed student's t-test: * $p < 0.05$, ** $p < 0.01$, and *** $p < 0.001$ CHIP vs IgG per concentration).

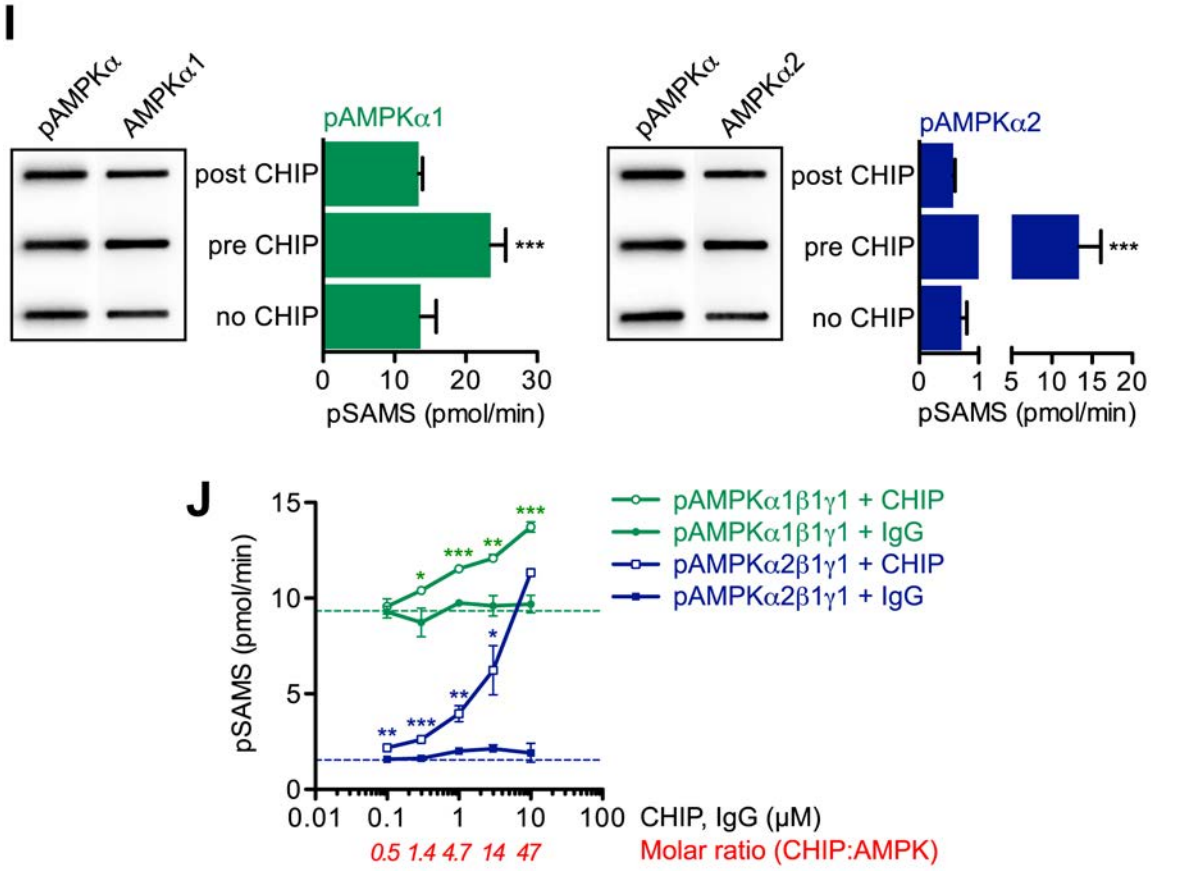

Supplemental Figure 4 I-J

Schisler *et al.*

Supplementary Figure 5 – Limited proteolysis and AMPKα2 twisted FRET functional analysis. (**A**) Limited proteolysis analysis of activated (phosphorylated αT172) pAMPKα2β1γ1 in the presence of either luciferase or CHIP, using increasing concentrations of proteinase K (PK) was analyzed via SDS-PAGE/immunoblot analysis to detect the proteolytic fingerprint of either AMPKα (top, white arrow) or AMPKγ (bottom, green arrow). The black arrows indicate a non-specific detection of PK. (**B**) COS7 cells were transfected with either the control (SGLRSRA) or AMPKα2 twisted FRET vector as indicated. The FRET protein products were immunoprecipitated (IP) using a GFP antibody and the association of FRET proteins with various AMPK subunits was detected via immunoblot analysis. The input lanes were 10% of the total amount of protein used in the immunoprecipitation (125 μg). Only the AMPKα2 twisted FRET protein co-immunoprecipitated with the other AMPK subunits expressed in COS7 cells demonstrating that the AMPKα2 twisted FRET vector is incorporated into AMPK holoenzyme complexes. The red, white, and black arrows indicate the AMPKα2 twisted FRET protein, control FRET protein, and endogenous AMPKα2 protein, respectively. (**C**) COS7 cells were transfected with either the control (SGLRSRA) or AMPKα2 twisted FRET vector in the presence or absence of CHIP co-expression as indicated. The FRET protein products were immunoprecipitated (IP) using a GFP antibody and the association of FRET vectors with CHIP was detected via immunoblot analysis. The input lanes were 10% of the total amount of protein used in the immunoprecipitation (125 μg). CHIP protein co-immunoprecipitated only with the AMPKα2 twisted FRET protein and not the control FRET protein. (**D**) COS7 cells were transfected with either the control (SGLRSRA) or AMPKα2 twisted FRET vector as indicated. 18 h after transfection, cells were treated with H_2O_2 (500 μM) for 30 m. The FRET protein products were immunoprecipitated (IP) using a GFP antibody or rabbit IgG as a negative control. Oxidative stress (H_2O_2)-mediated activation of endogenous AMPKα and the AMPKα2 twisted FRET protein was measured via immunoblot analysis using a pAMPKα-T172 antibody. (**E**) AMPK activity was measured by SAMS peptide phosphorylation (pSAMS) in the GFP-immune-complexes shown in (**D**). Reactions containing either the control FRET protein or the IgG

control immunoprecipitant had no detectable SAMS phosphorylation. Data are expressed as mean ± SEM from three biological replicates per condition (significant by student's t-test: ** $p < 0.01$ comparing the AMPKα2 twisted FRET protein in the presence vs. absence of H_2O_2, nd = not detected).

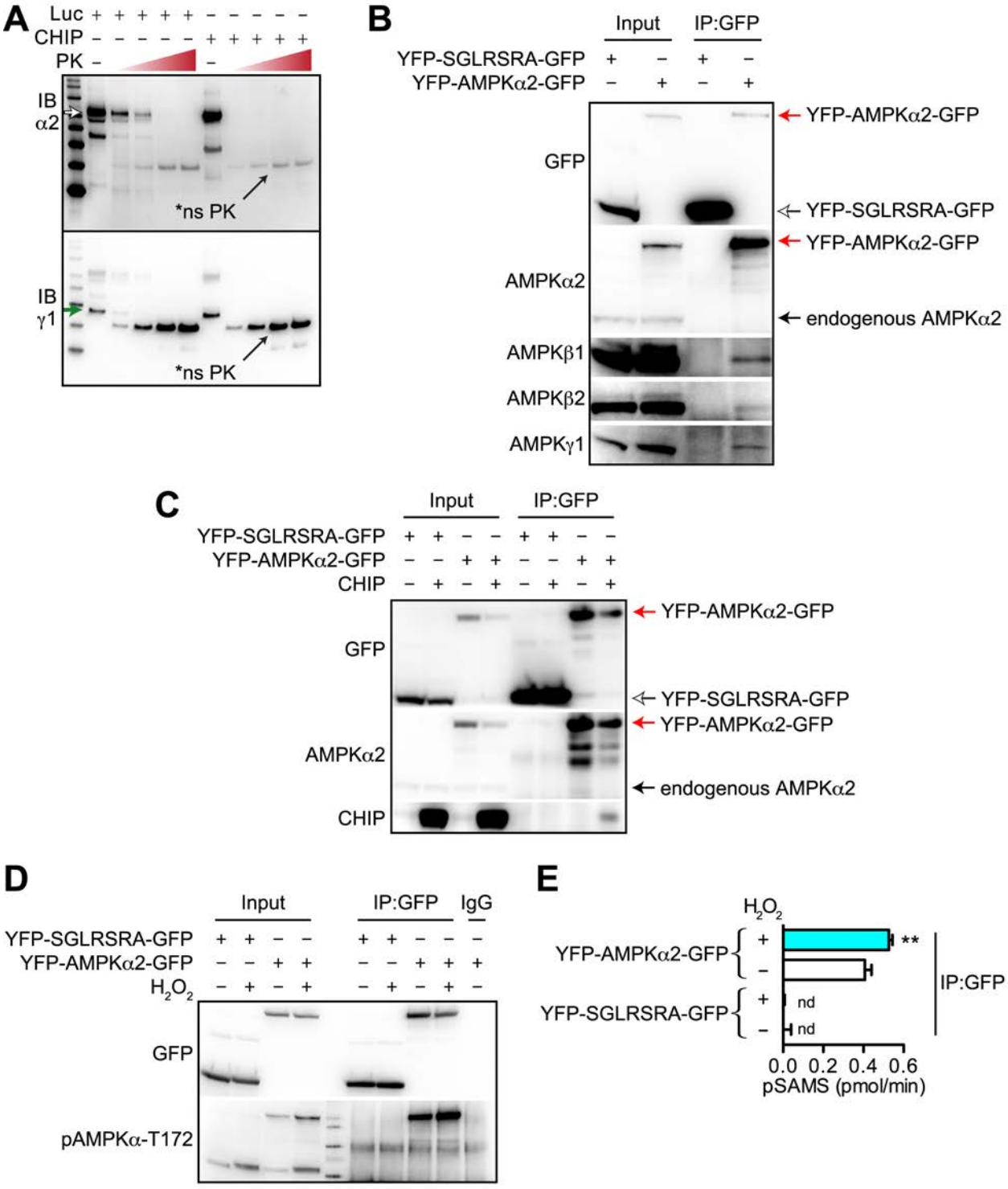

Supplemental Figure 5 A-E

Schisler *et al.*

Supplemental Tables

	Baseline		1 w TAB	
	Wild-type	*CHIP* $^{-/-}$	Wild-type	*CHIP* $^{-/-}$
*Body Weight (g)	19.7 ± 0.4	21.1 ± 0.6	19.3 ± 0.7	17.7 ± 0.6 ##
Heart rate (bpm)	605.2 ± 27.6	585.6 ± 30.2	711.9 ± 15.0 #	611.5 ± 40.6
**AWT;*d* (mm)	0.93 ± 0.03	0.95 ± 0.03	1.20 ± 0.04 ##	1.53 ± 0.08 ###,†††
AWT;*s* (mm)	1.60 ± 0.07	1.71 ± 0.06	1.87 ± 0.05 #	2.04 ± 0.09 ##
LVED;*d* (mm)	2.90 ± 0.06	3.28 ± 0.07 †	2.65 ± 0.10	2.70 ± 0.15 ###
LVED;*s* (mm)	1.13 ± 0.04	1.33 ± 0.07	1.00 ± 0.08	1.53 ± 0.16 ††
*PWT;*d* (mm)	0.90 ± 0.06	0.93 ± 0.04	1.06 ± 0.05	1.47 ± 0.12 ###,†††
*PWT;*s* (mm)	1.49 ± 0.03	1.60 ± 0.03	1.60 ± 0.06	2.01 ± 0.13 ###,†††
**%SF	61.1 ± 1.6	59.5 ± 1.8	62.7 ± 2.1	43.6 ± 4.1 ###,†††

Supplementary Table 1 – Echocardiography after one week of surgery. Left ventricular dimension data obtained via conscious echocardiography. When applicable, measurements reported at diastole or systole (*d* or *s* respectively); g, grams; bpm, beats per minute; mm, millimeters; AWT, anterior wall thickness; LVED, left ventricular end dimension; PWT, posterior wall thickness. Variables identified as significant via 2-way ANOVA on the interaction between genotype and surgery are defined as * $p < 0.05$ and ** $p < 0.01$. Bonferroni post-tests were used to identify significant differences comparing baseline and 1 w TAB: # $p < 0.05$, ## $p < 0.01$, and ### $p < 0.0001$; as well as differences comparing the wild-type and *CHIP* $^{-/-}$ genotype: † $p < 0.05$, †† $p < 0.01$, and ††† $p < 0.0001$.

Supplementary Table 2 (excel file – Supplementary Table 2.xls) – Microarray analysis of differential gene expression. A total of 168 microarray probes were identified as differentially expressed via 2-way AVOVA analysis with a corrected $p < 0.05$. Provided are the Agilent probe identifiers, corrected *p* value, the fold change and direction of change for the indicated group comparisons, gene symbol, Genbank accession, and gene description. In addition, the K-mean cluster for each gene is also provided and color coded to match the clusters as shown in Figure 2.

	Sham		1 w TAB	
Reference gene	Wild-type	*CHIP* $^{-/-}$	Wild-type	*CHIP* $^{-/-}$
Actb	1.03 ± 0.20	1.04 ± 0.08	1.06 ± 0.15	0.96 ± 0.06
GAPDH	1.11 ± 0.02	1.07 ± 0.12	0.81 ± 0.04	1.07 ± 0.04
Gusb	1.08 ± 0.13	0.91 ± 0.03	1.06 ± 0.12	1.01 ± 0.04
r18S	1.02 ± 0.03	0.99 ± 0.06	0.99 ± 0.04	1.03 ± 0.02
Tbp	1.08 ± 0.06	0.97 ± 0.04	0.96 ± 0.08	1.01 ± 0.05

Supplementary Table 3 – Reference gene expression levels determine by qPCR: The ΔCq values of the indicated reference gene measured in each condition are represented by the mean ± SEM from four biological replicates.

Reference gene	All samples	Genotype	Surgery
r18S	0.054	0.023	0.031
Tbp	0.051	0.023	0.020
Gusb	0.128	0.043	0.052
GAPDH	0.197	0.068	0.073
Actb	0.195	0.071	0.073
Best gene	*Tbp*	*r18S*	*Tbp*
Stability value	0.051	0.023	0.020
Best combination of two genes		*r18S* and *Tbp*	*r18S* and *Tbp*
Stability value		0.016	0.019

Supplementary Table 4 – Reference gene analysis for qPCR: Normfinder (3) was used to determine the stability values of five different candidate reference genes for qPCR analysis. The stability value of each gene was measured without any classification (*all samples*) or classified based on either *genotype* (wild-type vs *CHIP* $^{-/-}$) or *surgery* condition (Sham vs TAB). Independent of the different classifications, *Tbp* and *r18S* were the most stable genes across all samples; therefore, the geometric mean of *Tbp* and *r18S* were used to normalize qPCR expression values.

	Sham		1 w TAB	
	Wild-type	*CHIP* $^{-/-}$	Wild-type	*CHIP* $^{-/-}$
ATP (nmol/mg)	3.27 ± 0.29	5.76 ± 1.21	6.20 ± 1.20 †	5.20 ± 0.31
ADP (nmol/mg)	1.11 ± 0.01	1.71 ± 0.21 †	1.97 ± 0.04 ##	2.27 ± 0.10 #
ADP:ATP	0.34 ± 0.02	0.32 ± 0.03	0.33 ± 0.04	0.44 ± 0.02 †

Supplementary Table 5 – Adenine nucleotide levels from mouse hearts. Total ATP and ADP levels (nmol/mg) and ratios were measured as described in the Extended Experimental Procedures. 2-way ANOVA post-tests used to identify significant differences comparing sham and 1 w TAB: # $p < 0.05$ and ## $p < 0.01$; as well as differences comparing the wild-type and *CHIP* $^{-/-}$ genotype: † $p < 0.05$.

Protein	ng/mg	Mass (kd)	nmoles/g	Molar ratio (CHIP:protein)
STUB1 (CHIP)	7.47	35	213	N/A
PRKAA2 (AMPKα2)	4.24	62	68.4	3.1 : 1
PRKAB2 (AMPKβ2)	6.59	30	219	1.0 : 1
PRKAG1 (AMPKγ1)	25.33	38	667	0.3 : 1
PRKAG2 (AMPKγ2)	3.32	63	53	4.1 : 1

Supplementary Table 6 – Stoichiometry of CHIP:AMPK subunits in human heart. The amount of protein per mg of heart tissue was adapted from Aye *et al.* (4). The amount of each protein (nmoles/g) was calculated using the predicted mass of each species as provided in the UniProt database (5). The stoichiometry of CHIP:AMPK for each subunit is provided. This analysis demonstrates that within the heart, CHIP protein exists in over a 3:1 molar excess of AMPKα2 (the predominant α isoform in the heart). This ratio remains the same even if we factor in intact AMPK holoenzymes (αβγ) as AMPKα2 (PRKAA2) is the limiting component of the holoenzyme in the heart.

Supplementary Table 7 (excel file – Supplementary Table 7.xls) – Protein sequence distribution of limited proteolysis of pAMPKα2β1γ1 in the presence of CHIP. Proteins were identified using Matrix-assisted laser desorption/ionization time of flight/time of flight mass spectrometry (MALDI TOF/TOF MS). The top scoring protein match for each band is provided (on separate worksheets) including the peptide sequences and overall coverage of the matching protein.

Extended Experimental Procedures

Animal Studies. We bred an inbred *CHIP* $^{-/-}$ 129SvEv mouse strain by repeatedly backcrossing the 129SvEv mouse strain (Charles River) with 129Sv/C57B6 mice carrying a single mutated *CHIP* allele (6). The resulting offspring are 25% *CHIP* $^{-/-}$ and 25% *CHIP* $^{+/+}$; therefore, all animals used are equally backcrossed as we use littermate controls. The age of *CHIP* $^{-/-}$ mice and wild-type littermates used throughout the studies ranged from 8-12 weeks. All procedures complied with NIH standards for the care and use of animal subjects and were approved by the Institutional Animal Care and Use Committee. To induce pressure overload cardiac hypertrophy, mice were subjected to transverse aortic banding (TAB) as described (7) using Doppler analysis to ensure physiologic constriction of the aorta. Doppler flow velocity ratios between right and left carotid artery (RC/LC) in our TAB procedures ranged between 6-9. Sham-operated mice underwent the same procedure except for aortic constriction. We performed conscious echocardiography using two-dimensional and M-mode imaging using a Vevo 660 ultrasound system (VisualSonics) as previously described (8). For *in vivo* aminoimidazole carboxamide ribonucleotide (AICAR) treatment, either AICAR (250 mg kg^{-1}) or an equivalent volume of saline was administered via intraperitoneal injections every 24 hours for a total of three administrations as described (9).

Primary mouse neonatal ventricular cardiomyocyte isolation: Primary neonatal mouse ventricular cardiomyocytes were isolated from one-day-old mouse neonates utilizing the Worthington Cardiomyocyte Isolation System and manufacturer's instructions, with the following modifications. After collagen digestion and filtration, cells were pelleted at 1000 x *g* for 5 m at room temperature and the supernatant collected. This supernatant was plated for 2 h at 37 °C, 5% CO_2, allowing non-myocyte cells to adhere. After 2 h, the supernatant containing the cardiomyocytes, which had not yet adhered, were collected and re-plated in a separate cell culture dish in fresh DMEM containing 10% horse serum, 5% fetal bovine serum, 100 IU

penicillin-100 μg ml^{-1} streptomyocin and 100 μM 5-bromo-2'-deoxyuridine to prevent non-myocyte cell growth. Fresh DMEM containing 10% fetal bovine serum and 100 IU penicillin-100 μg ml^{-1} streptomycin was then added to the plate containing non-myocyte cells. Both the myocyte and non-myocyte cultures were maintained at 37 °C, 5% CO_2 for 72 h, replacing the media with fresh media every 24 h post-plating.

Histology. Mouse hears were perfused, processed for histology, and stained with either hematoxylin and eosin for routine histological examination, Masson's trichrome for collagen, or oil red O for neutral lipids. Sarcolemmal membranes were identified with Triticum vulgaris lectin TRITC conjugate staining and used to quantify cardiomyocyte cross-sectional area via fluorescence microscopy performed as described (10). ImageScope software (Aperio®) was used to calculate the percent interstitial fibrosis using whole heart sections stained with Masson's trichrome. The ventricle area of each section was selected and image color processing was used to calculate the amount area of fibrosis relative to the total tissue area.

Electron microscopy of myocardium and mitochondrial volume density analysis. Cardiac muscle fragments were fixed with 2% glutaraldehyde in 0.1 M phosphate buffer (pH 7.4), postfixed in 1% osmic acid for 1 h, and photographed in a JEOL 1200 EX electron microscope (JEOL USA). Mitochondrial volume density was calculated using the point counting grid method as described only on micrographs with tangential cuts where the muscle fibers are viewed in a longitudinal plane (11). The measurements obtained by this method from our electron micrographs of wild-type sham hearts were consistent with the reported mitochondrial volume density for normal heart tissue (11) of 0.39 μm^{-3} μm^{-3}.

Indirect immunofluorescence. Paraformaldehyde-fixed, paraffin-embedded sections of mouse hearts were used for indirect immunofluorescent detection of either CHIP or the cardiomyocyte marker cardiac troponin C using the antibodies indicated in the antibody table (see below). Slides

were deparraffinized and hydrated. Antigen retrieval was performed with 10 mM sodium citrate buffer (pH 6) with tween-20 (0.02%) for 3 m in the microwave and repeated with fresh buffer two more times. All antibody incubations were done sequentially for 1 h diluted in 10% fetal calf serum. Images were acquired on an inverted DMIRB microscope (Leica) with an OcraER camera (Hamamatsu) and processed using Photoshop CS5 (Adobe). Mismatched secondary controls and images on *CHIP* $^{-/-}$ heart sections were acquired using identical acquisition settings.

Expression and qPCR analyses. For microarray analysis, cyanine-5-labeled cRNA was co-hybridized to the G4122F mouse whole genome array (Agilent) with equimolar amounts of cyanine-3-labeled mouse reference RNA (12). Complete, MIAME-compliant datasets are archived with the Gene Expression Omnibus of the National Center for Biotechnology Information and are accessible through the GEO Series accession record GSE24209. 14,322 probes were identified as present or marginal in at least 50% of the biological replicates in one of the four conditions and used for PCA, 2-way ANOVA, and K-means clustering (Agilent GeneSpring GX 11.5). Functional enrichment on gene clusters determined the fold enrichment using the Database for Annotation, Visualization and Integrated Discovery (DAVID) (13). Relative mRNA analysis was performed by reverse transcribing total RNA into cDNA using the iScript cDNA Synthesis Kit (Bio-Rad) followed by quantitative real-time PCR (qPCR) on 5 ng of cDNA using either the 7900 HT sequence detection system (Life Technologies) or LightCycler 480 (Roche) with corresponding software and reagents; see following table for gene-specific assay information. Relative expression values were calculated using the ΔCT method correcting for PCR efficiency and mean centered across the four experimental conditions. Expression was normalized to the geometric mean of *r18S* and *Tbp,* the two most stable reference genes across genotypes and surgery conditions as determined via Normfinder (3) (Supplementary Table 3, Supplementary Table 4 and Supplementary Figure 3, also tested *Gapdh, Actb*, and *Gusb*). Relative mitochondrial number was determined by performing qPCR on 2 ng of isolated DNA from whole heart homogenate using three mitochondrial gene targets,

CYTB, *ND1*, *COX*. Relative content was mean centered across the four experimental conditions and normalized to the *H19* genomic DNA target as an endogenous control as previously described (14).

Assay information for qPCR.

Gene targets and nucleic acid type for qPCR assays with corresponding chemistry and primer sequences (if applicable). For assays that use probe-based chemistry, the corresponding UniversalProbe Library number (UPL, Roche Applied Science) or TaqMan® Gene Expression Assay (Life Technologies™) identifier is listed.

Target	Type	Chem	Primer 1	Primer 2	Probe
Actb	mRNA	5' exo	ctaaggccaaccgtgaaaag	accagaggcatacagggaca	UPL #64
Atp5a1	mRNA	5' exo	tccatgcctctaacactcgac	gacgtgtcagctcccagaa	UPL #91
Atp5g3	mRNA	5' exo	gtcgcctgtcacctagatcc	tgcagaaattggtctatatgcaa	UPL #72
CYTB	mRNA	5' exo	catttattatcgcggcccta	tgggttgtttgatcctgtttc	UPL #69
Gusb	mRNA	5' exo	ctctggtggccttacctgat	cagttgttgtcaccttcacctc	UPL #42
Ndufa5	mRNA	5' exo	agggtggtgaagtggaagag	tggccacttccactggtta	UPL #31
Ndufaf4	mRNA	5' exo	tgagaagaatccagcgatga	cagtcacctcccatctttgc	UPL #16
Ndufb10	mRNA	5' exo	agcctaccaggaccgctac	tggaatgaagagttctggtcac	UPL #51
Ndufb9	mRNA	5' exo	tccaagagagagcagtggaag	ctcctgcagctgcttaacct	UPL #33
Ndufs4	mRNA	5' exo	gatgggaaaatcctttgatgg	gaaggtcagaaccatgttgga	UPL #105
Ndufs7	mRNA	5' exo	gtggtgaccaagctggatg	cgaaggtcataggccacag	UPL #104
TBP	mRNA	5' exo	cggtcgcgtcattttctc	gggttatcttcacacaccatga	UPL #107
Acox1	mRNA	5' exo			Mm00443579_m1
Ppargc1a	mRNA	5' exo			Mm00447183_m1
Ppara	mRNA	5' exo			Mm00440939_m1
18S	rRNA				4319413E
Gadd45	mRNA	SYBR	tgctactggagaacgacgc	ggatccttccattgtgatgaa	
Gapdh	mRNA	SYBR	acccagaagactgtggatgg	cacattgggggtaggaacac	
Cdkn1b	mRNA	SYBR	agtgtccagggatgaggaag	ggggaaccgtctgaaacatt	
Sod2	mRNA	SYBR	actgaagttcaatggtgggg	gcttgatagcctccagcaac	
H19	gDNA	SYBR	gtacccacctgtcgtcc	gtccacgagaccaatgactg	
ND1	mtDNA	SYBR	aatcgccatagccttcctaacat	ggcgtctgcaaatggttgtaa	
CYTB	mtDNA	SYBR	ttctgaggtgccacagttatt	gaaggaaaggtattaagggctaaa	
COX1	mtDNA	SYBR	cccaatctctaccagcatc	ggctcatagtatagctggag	

Adenine nucleotide measurements from heart tissue. Hearts were flash frozen and 50-100 mg of tissue was homogenized in ice cold 0.4 M perchloric acid with 0.5 mM EGTA. Samples were incubated on ice for 5 m and centrifuged at 3200 x *g* at 4 °C for 10 m. The supernatants were moved to clean pre-chilled tubes and 0.5 M K_2CO_3 was added to a final concentration of 125 mM to neutralize the acid. Final concentration of the samples were 75 mg ml^{-1}. Samples were mixed, incubated on ice for 5 m and centrifuged at 3200 x *g* at 4 °C for 5 m. The supernatants were transferred to clean pre-chilled tubes and frozen until analyzed. Cardiac ATP and ADP concentrations were measured using an HPLC method using calibrated standards. Separation is achieved within 30 minutes using a LC18-T chromatography column. Detection is carried out using a Waters 490 UV detector. Nucleotide measurements were similar to other published values including mice on the 129Sv background (15, 16).

Polyacrylamide gel electrophoresis, immunoblotting, and densitometry. For reduced and denatured conditions, protein samples were resolved on NuPAGE Novex® Bis-Tris Gels (Life Technologies) using the MOPS/LDS buffer system. Native protein samples were resolved on 4-16% NativePAGE Novex® Gels (Life Technologies) using 0.001% G-250 cathode buffer. Two-dimensional native-SDS-PAGE was performed using the combination of these two systems per the manufacturer's instructions. Proteins were transferred to PVDF membranes and incubated with primary antibodies overnight (see following table for antibody information) and detected with either anti-rabbit or anti-mouse (GE Healthcare), or anti-goat (Sigma) HRP-conjugated antibodies and visualized with ECL Advance substrate (GE Healthcare) using the EC3™ Imaging System (UVP). For quantification of relative protein levels, densitometry analysis was performed using FIJI (NIH) (17). For visualization of proteins, gels were stained with either coomassie brilliant blue G-250 or SYPRO® ruby.

Antibody information

Vendor	Catalog#	Target	Dilution
Cell Signaling	2080	CHIP	1:1000
Cell Signaling	2532	AMPKα	1:1000
Cell Signaling	2534	AMPKγ2	1:1000
Cell Signaling	3661	Phospho-Acetyl-CoA Carboxylase-Ser79	1:1000
Cell Signaling	4148	AMPKβ2	1:1000
Cell Signaling	4182	AMPKβ1	1:1000
Cell Signaling	4187	AMPKγ1	1:1000
Cell Signaling	4188	Phospho-AMPKα-Thr172	1:2000
Cell Signaling	4872	HSP70	1:1000
Cell Signaling	4874	HSP90	1:1000
Cell Signaling	9271	Phosho-AKT-Ser473	1:1000
Cell Signaling	9272	AKT	1:1000
Cell Signaling	9452	4E-BP1	1:1000
Cell Signaling	9455	Phospho-4E-BP1-Thr70	1:1000
GE Healthcare	27-4577-01	GST	1:1000
GE Healthcare	NA931	Mouse IgG-HRP	1:60000 - 1:200000
GE Healthcare	NA934	Rabbit IgG-HRP	1:60000 - 1:200000
Life Technologies	A21131	Mouse IgG2a	1:100 (IF)
Life Technologies	A21143	Mouse IgG2b	1:100 (IF)
Millipore	05-832	LKB1	1:500
Millipore	07-315	SGK1	1:1000
Millipore	07-662	ERRα	1:1000
Millipore	36-002	pSGK1	1:1000
R&D Systems*	AF2850	AMPKα2	1:5000
R&D Systems*	AF3197	AMPKα1	1:5000
SantaCruz Biotech*	Sc-8185	LKB1 (N-19)	
Sigma-Aldrich®	A5420	Goat IgG-HRP	1:60000 - 1:200000
Sigma-Aldrich®	A5441	β-ACTIN	1:5000
Sigma-Aldrich®	G6795	GFP	1:1000
Sigma-Aldrich®	G8795	GAPDH	1:10000
Sigma-Aldrich®*	I5006	Rabbit IgG	As described
Sigma-Aldrich®*	I5256	Goat IgG	As described
Sigma-Aldrich®*	I5381	Mouse IgG	As described
Sigma-Aldrich®*	S1073	CHIP	1:5000, 1:100 (IF)
Sigma-Aldrich®	T8328	β-TUBULIN	1:5000
abcam*	ab290	GFP	1:100
abcam	ab8285	Cardiac troponin C (TnC)	1:50 (IF)

* indicates antibodies used in immunoprecipitations

5'-AMP-activated Protein Kinase (AMPK) and LKB1 activity, phosphorylation, and dephosphorylation assays. Analyses of AMPK and LKB1 activity in tissue samples were performed using immuno-isolation of either AMPKα1-, AMPKα2-, or LKB1-containing complexes. Immuno-isolation of total AMPKα or GFP was used to measure AMPK activity in cell lines. The antibodies used for immunoprecipitations are indicated in the Antibody Information table above. AMPK activity was determined by measuring the amount of ^{33}P-labeled phosphate incorporated into synthetic SAMS peptide (HMRSAMSGLHLVKRR) in the presence of 200 μM AMP for 20 min at 30 °C with constant shaking as described (18). LKB1 activity was measured in the same conditions using the LKBtide peptide (LSNLYHQGKFLQTFCGSPLYRRR) as substrate. To assay AMPKα-T172 phosphorylation, all reactions were performed at 30 °C as described (19, 20). Recombinant monomeric inactive AMPKα2 (15 μg ml^{-1}), AMPKα1β1γ1 (100 μg ml^{-1}), or AMPKα2β1γ1 (100 μg ml^{-1}) were incubated in 10 μl of Buffer A (20 μM HEPES, 10 μM KCl) for 30 min at 30 °C in the presence or absence of recombinant CHIP, CHIP-K30A, and CHIPΔU-box (final concentration = 6 μM for monomeric AMPKα2, 2 μM or AMPK holoenzymes). Kinase reactions were started by the addition purified and active LKB1/STRADα/MO25α at one-tenth of the concentration of AMPK in the reaction a final volume of 35 μl in Buffer B (50 mM Tris/HCl pH 7.5, 0.1 mM EGTA, 5 mM magnesium acetate, 0.1% β-mercaptoethanol, and 0.1 mM ATP). Aliquots were removed at the indicated time points using 50 mM EDTA to quench the kinase reaction and the quenched reaction was used for SDS-PAGE/immunoblot analysis. Two μl of the quenched reaction was used for AMPK activity assays. Dephosphorylation of activated (phosphorylated α-T172) pAMPK holoenzymes (31.3 μg ml^{-1}) were performed in dephosphorylation buffer (50 mM MOPS pH 7, 100 mM NaCl, 0.1 mM EDTA, and 2.5 mM MgCl2) in the presence or absence of CHIP (2 μM), AMP (0.2 mM), or PP2Cα (0.4 μM) as described (21). AMPK activity was measured in purified protein samples assayed using the SAMS peptide as previously described (18).

Immunoprecipitations. All immunoprecipitations (IPs) were performed using Dynabeads® Protein G (Life Technologies). **Mouse heart IPs**: beads (50 µl beads/IP) were cleared with PBS-T (0.01% Tween 20) and conjugated at 25 °C for 10 min with either 2 µg (AMPKα1 or AMPKα2 goat polyclonal antibodies, or goat IgG) or 5 µg (CHIP mouse monoclonal antibody or mouse IgG). Heart lysate samples were first cleared with 50 µl of unconjugated beads incubated with rotation for 10 m at 4 °C. The unconjugated beads were removed and 50 µl of each sample (200 µg of protein) was added to each antibody condition in a final volume of 300 µl (PBS-T) and incubated with rotation for 1 h at 4 °C. Reactions were washed once with PBS-T and incubated with rotation for 10 m at 4 °C followed by four more washes with PBS-T. The samples were moved to clean tubes to eliminate and non-specific binding to the tubes, and the bound proteins were removed by the addition of LDS loading buffer containing reducing agent (Life Technologies) for 10 min at 70 °C and resolved via SDS-PAGE/immunoblot analysis. **Recombinant protein IPs**: recombinant CHIP (0.72 µM) or AMPK holoenzyme (0.36 µM) were incubated alone or together (at a molar ratio 2:1, respectively) for 30 min at 30 °C. The reactions were then added to beads pre-conjugated with either 1 µg of AMPKα1 or AMPKα2 goat polyclonal antibody or CHIP mouse monoclonal antibodies in a final volume of 300 µl (PBS) and incubated with rotation for 15 min at 25 °C. Bound proteins were removed after eight washes with PBS-T and resolved as described above.

Cell culture, expression plasmids, and recombinant proteins. COS7 cells and SV40-transformed mouse embryonic fibroblasts isolated from either wild-type or *CHIP* $^{-/-}$ mice were cultured in DMEM with 10% serum as previously described (22). The rat cDNA encoding *AMPKα2* (Addgene) was cloned in frame with an N-terminal ECFP and C-terminal EYFP vector, kindly provided by Bakhrom Berdiev, University of Alabama at Birmingham (23). The positive control vector contained a seven amino acid linker (23) (SGLRSRA) in the place of AMPKα2. Expression vectors for CHIP, CHIP(K30A), CHIP(ΔU-box), and the recombinant adenoviruses expressing CHIP, CHIP(K30A) or GFP have been described previously (22). Cells were treated

with adenovirus at a multiplicity of infection (MOI) of 25 virus particles per cell for 18 h, then exposed to 250 μM H_2O_2 for 15 min. His-tagged constructs for AMPKα1β1γ1 and AMPKα2β1γ1 were kindly provided by Dietbert Neumann, ETH Zurich, Switzerland (24); His-tagged constructs for CHIP, CHIP(K30A), and CHIP(ΔU-box) were used as described previously (1, 25). Proteins were produced in Escherichia coli BL21(DE3) followed by purification with HisTrap™ HP columns (GE Healthcare) and further purification via gel filtration chromatography using either HiLoad™ 16/60 Superdex™ 75 or 200 prepgrade columns. Activated (phosphorylated α-T172) pAMPK was prepared by incubating α1- or α2-containing holoenzymes with CAMKK2 (Sigma-Aldrich®) at a 100:1 ratio respectively in CAMKK2 buffer consisting of 50 mM Tris pH 8, 100 mM NaCl, 10 mM MgCl2, 2 mM DTT, and 1 mM ATP, incubated at 25 °C for 1 h as described (21). The CAMKK2 was removed by immunoprecipitation using MagneGST™ beads (Promega). Additional experiments were carried out using PP2Cα (GenWay), LKB1/MOD25α/STRADα (Sigma-Aldrich®), AMPKα2 (Abnova), activated (phosphorylated α-T172) pAMPKα1β1γ1 (Cell Signaling), activated (phosphorylated α-T172) pAMPKα2β1γ1 (Cell Signaling), and firefly luciferase (Roche).

Size exclusion chromatography and multi angle light scattering (SEC-MALS). 100 μl of recombinant protein samples (single proteins used at 1 mg ml^{-1}, combination of AMPKα2β1γ1 and CHIP used at 1 mg ml^{-1} and 0.5 mg ml^{-1}, respectively) were separated using a 10/300 Superdex™ 200 GL column using an FPLC system (Agilent) interfaced with a DAWN HELEOS II light scattering instrument (Wyatt), T-rEX refractometer (Wyatt), dynamic light scattering module (Wyatt), and Eclipse asymmetric fixed flow fractionator (Wyatt). Relative Rayleigh ratios were used for overlays of the chromatographs.

Limited proteolysis of AMPK holoenzyme and peptide sequencing. Activated (phosphorylated α-T172) pAMPKα2β1γ1 (10 μg ml^{-1}) was incubated alone or in the presence of 3.8 μg of luciferase or CHIP for 30 min at 30 °C then digested with trypsin (1, 2, 3, 5 μg ml^{-1}) or proteinase (PK, 1,

5, 10, 20 μg ml^{-1}) in digestion buffer (150 mM KCl, 25 mM Hepes, pH 7.4, and 10 mM DTT) for 1 h at 30 °C as previously described (26). Digestions were terminated with the addition of HALT™ Protease and Phosphatase Inhibitor Cocktail (Thermo Scientific). Protease-resistant fragments of pAMPK holoenzyme were analyzed by immunoblot analysis or SYPRO®-ruby as described above. For protein sequencing, selected bands were excised and digested in gel with trypsin. The resulting peptides were identified using an ABI 4800 Matrix-assisted laser desorption/ionization time of flight/time of flight mass spectrometer (MALDI TOF/TOF MS, Life Technologies). Mascot software (Matrix Science) was used to identify the top scoring protein match for each band.

Twisted FRET assay. Acceptor photobleaching fluorescent resonance energy transfer (AP-FRET) (27) was used with the twisted FRET (double-tagged ECFP-EYFP) method as previously described (23, 28) to quantify changes in AMPKα2 protein conformational changes in live cells. Images were acquired using a Zeiss 510 Laser Scanning Confocal Microscope using a 63x 1.4 aperture plan-Apochromat objective using the 488 and 514 nm laser lines to excite ECFP (donor) and EYFP (acceptor) fluorescence, respectively. Emission spectra for ECFP and EYFP were collected using 465-500 and 525-600 nm bandpass filters, respectively. Whole cell photobleaching was accomplished using the 514 nm laser to photobleach the acceptor to 30-35% of the original intensity. Apparent FRET efficiency (E) was calculated using emission spectra before and after photobleaching (D_{pre} and D_{post}, respectively) from five equal regions (20 pixel radius) per cell encompassing regions of double fluorescence using the Zeiss software and the equation: $E = (D_{post} - D_{pre})/D_{post}$ corrected for bleaching efficiency as described (29).

Supplemental References

1. Rosser, M.F., Washburn, E., Muchowski, P.J., Patterson, C., and Cyr, D.M. 2007. Chaperone functions of the E3 ubiquitin ligase CHIP. *J Biol Chem* 282:22267-22277.
2. Scholz, R., Suter, M., Weimann, T., Polge, C., Konarev, P.V., Thali, R.F., Tuerk, R.D., Viollet, B., Wallimann, T., Schlattner, U., et al. 2009. Homo-oligomerization and activation of AMP-activated protein kinase are mediated by the kinase domain alphaG-helix. *The Journal of biological chemistry* 284:27425-27437.
3. Andersen, C.L., Jensen, J.L., and Orntoft, T.F. 2004. Normalization of real-time quantitative reverse transcription-PCR data: a model-based variance estimation approach to identify genes suited for normalization, applied to bladder and colon cancer data sets. *Cancer Res* 64:5245-5250.
4. Aye, T.T., Scholten, A., Taouatas, N., Varro, A., Van Veen, T.A., Vos, M.A., and Heck, A.J. 2010. Proteome-wide protein concentrations in the human heart. *Mol Biosyst* 6:1917-1927.
5. UniProt, C. 2012. Reorganizing the protein space at the Universal Protein Resource (UniProt). *Nucleic Acids Res* 40:D71-75.
6. Dai, Q., Zhang, C., Wu, Y., McDonough, H., Whaley, R.A., Godfrey, V., Li, H.H., Madamanchi, N., Xu, W., Neckers, L., et al. 2003. CHIP activates HSF1 and confers protection against apoptosis and cellular stress. *EMBO J* 22:5446-5458.
7. Hu, P., Zhang, D., Swenson, L., Chakrabarti, G., Abel, E.D., and Litwin, S.E. 2003. Minimally invasive aortic banding in mice: effects of altered cardiomyocyte insulin signaling during pressure overload. *Am J Physiol Heart Circ Physiol* 285:H1261-1269.
8. Collins, K.A., Korcarz, C.E., and Lang, R.M. 2003. Use of echocardiography for the phenotypic assessment of genetically altered mice. *Physiol Genomics* 13:227-239.
9. Zou, M.H., Kirkpatrick, S.S., Davis, B.J., Nelson, J.S., Wiles, W.G.t., Schlattner, U., Neumann, D., Brownlee, M., Freeman, M.B., and Goldman, M.H. 2004. Activation of the

AMP-activated protein kinase by the anti-diabetic drug metformin in vivo. Role of mitochondrial reactive nitrogen species. *J Biol Chem* 279:43940-43951.

10. Willis, M.S., Ike, C., Li, L., Wang, D.Z., Glass, D.J., and Patterson, C. 2007. Muscle ring finger 1, but not muscle ring finger 2, regulates cardiac hypertrophy in vivo. *Circulation research* 100:456-459.
11. Medeiros, D.M. 2008. Assessing mitochondria biogenesis. *Methods* 46:288-294.
12. He, X.R., Zhang, C., and Patterson, C. 2004. Universal mouse reference RNA derived from neonatal mice. *Biotechniques* 37:464-468.
13. Huang da, W., Sherman, B.T., and Lempicki, R.A. 2009. Systematic and integrative analysis of large gene lists using DAVID bioinformatics resources. *Nat Protoc* 4:44-57.
14. Hayashi, M., Imanaka-Yoshida, K., Yoshida, T., Wood, M., Fearns, C., Tatake, R.J., and Lee, J.D. 2006. A crucial role of mitochondrial Hsp40 in preventing dilated cardiomyopathy. *Nat Med* 12:128-132.
15. Ashrafian, H., Docherty, L., Leo, V., Towlson, C., Neilan, M., Steeples, V., Lygate, C.A., Hough, T., Townsend, S., Williams, D., et al. 2010. A mutation in the mitochondrial fission gene Dnm1l leads to cardiomyopathy. *PLoS Genet* 6:e1001000.
16. Watanabe, K., Fujii, H., Takahashi, T., Kodama, M., Aizawa, Y., Ohta, Y., Ono, T., Hasegawa, G., Naito, M., Nakajima, T., et al. 2000. Constitutive regulation of cardiac fatty acid metabolism through peroxisome proliferator-activated receptor alpha associated with age-dependent cardiac toxicity. *The Journal of biological chemistry* 275:22293-22299.
17. Schindelin, J., Arganda-Carreras, I., Frise, E., Kaynig, V., Longair, M., Pietzsch, T., Preibisch, S., Rueden, C., Saalfeld, S., Schmid, B., et al. 2012. Fiji: an open-source platform for biological-image analysis. *Nat Methods* 9:676-682.
18. Keyse, S.M. 2000. *Stress response : methods and protocols*. Totowa, N.J.: Humana Press. xvi, 488 p. pp.

19. Jaleel, M., Villa, F., Deak, M., Toth, R., Prescott, A.R., Van Aalten, D.M., and Alessi, D.R. 2006. The ubiquitin-associated domain of AMPK-related kinases regulates conformation and LKB1-mediated phosphorylation and activation. *Biochem J* 394:545-555.

20. Lizcano, J.M., Goransson, O., Toth, R., Deak, M., Morrice, N.A., Boudeau, J., Hawley, S.A., Udd, L., Makela, T.P., Hardie, D.G., et al. 2004. LKB1 is a master kinase that activates 13 kinases of the AMPK subfamily, including MARK/PAR-1. *EMBO J* 23:833-843.

21. Chen, L., Jiao, Z.H., Zheng, L.S., Zhang, Y.Y., Xie, S.T., Wang, Z.X., and Wu, J.W. 2009. Structural insight into the autoinhibition mechanism of AMP-activated protein kinase. *Nature* 459:1146-1149.

22. Qian, S.B., McDonough, H., Boellmann, F., Cyr, D.M., and Patterson, C. 2006. CHIP-mediated stress recovery by sequential ubiquitination of substrates and Hsp70. *Nature* 440:551-555.

23. Berdiev, B.K., Cormet-Boyaka, E., Tousson, A., Qadri, Y.J., Oosterveld-Hut, H.M., Hong, J.S., Gonzales, P.A., Fuller, C.M., Sorscher, E.J., Lukacs, G.L., et al. 2007. Molecular proximity of cystic fibrosis transmembrane conductance regulator and epithelial sodium channel assessed by fluorescence resonance energy transfer. *J Biol Chem* 282:36481-36488.

24. Neumann, D., Woods, A., Carling, D., Wallimann, T., and Schlattner, U. 2003. Mammalian AMP-activated protein kinase: functional, heterotrimeric complexes by co-expression of subunits in Escherichia coli. *Protein expression and purification* 30:230-237.

25. Meacham, G.C., Patterson, C., Zhang, W., Younger, J.M., and Cyr, D.M. 2001. The Hsc70 co-chaperone CHIP targets immature CFTR for proteasomal degradation. *Nat Cell Biol* 3:100-105.

26. Lu, Z., and Cyr, D.M. 1998. The conserved carboxyl terminus and zinc finger-like domain of the co-chaperone Ydj1 assist Hsp70 in protein folding. *J Biol Chem* 273:5970-5978.

27. Karpova, T.S., Baumann, C.T., He, L., Wu, X., Grammer, A., Lipsky, P., Hager, G.L., and McNally, J.G. 2003. Fluorescence resonance energy transfer from cyan to yellow fluorescent protein detected by acceptor photobleaching using confocal microscopy and a single laser. *J Microsc* 209:56-70.

28. Xu, H., Zhang, Z., Li, M., and Zhang, R. 2010. MDM2 promotes proteasomal degradation of p21Waf1 via a conformation change. *J Biol Chem* 285:18407-18414.

29. Trinkle-Mulcahy, L., Chusainow, J., Lam, Y.W., Swift, S., and Lamond, A. 2007. Visualization of intracellular PP1 targeting through transiently and stably expressed fluorescent protein fusions. *Methods Mol Biol* 365:133-154.